GEOFLUIDS

Geofluids (2015) doi: 10.1111/gfl.12159

Low-temperature dunite hydration: evaluating CH_4 and H_2 production from H_2O and CO_2

A. NEUBECK[1], D. T. NGUYEN[2] AND G. ETIOPE[3,4]

[1]*Department of Geological Sciences, Stockholm University, Stockholm, Sweden;* [2]*Earth Systems Research Center, Institute for the Study of Earth, Oceans and Space, Department of Earth Sciences, University of New Hampshire, Durham, NH, USA;* [3]*Istituto Nazionale di Geofisica e Vulcanologia, Rome, Italy;* [4]*Faculty of Environmental Science and Engineering, Babes-Bolyai University, Cluj-Napoca, Romania*

ABSTRACT

Abiotic methane (CH_4) and hydrogen (H_2) produced after hydration of mafic/ultramafic rocks represent energy sources for microbes that may thrive in the deep subsurface regions of Earth and possibly on other planets. While H_2 is a direct product of serpentinization, CH_4 can form via Fischer–Tropsch Type (FTT) reactions (carbon reduction) that, due to potential H_2 migration, can be spatially and temporally detached from serpentinization. We tested an alternative process hypothesized by some scholars, in which CO_2 can be reduced through dunite hydration without initially added H_2, implying that CH_4 can form in the same serpentinized fluid–rock system. The experiment used natural dunite sand (Forsterite 92), CO_2 with $\delta^{13}C \sim -25‰$ (VPDB), and a 1 mM dissolved SiO_2 solution mixed in 30 glass bottles (118 mL) stored for up to 8 months at low temperature (50°C) to simulate land-based serpentinization systems. In addition, 30 control bottles without olivine were used as blanks. Trivial amounts of CH_4 (orders of 0.2–0.9 ppmv) were detected in both samples and blanks, likely representing analytical noise; essentially, no significant amount of CH_4 formed under the experimental conditions used in this work. Low amounts of H_2 (~2.55 ± 1.39 ppmv) were generated, with production yields that were one order of magnitude lower than in previously published experiments. Moderate concentrations of SiO_2 appeared to hinder low-temperature H_2 production. Our experiment confirms that the low-temperature reduction of CO_2 into CH_4 through direct olivine hydration, without initial H_2, is sluggish and not straightforward, which is consistent with previous studies. The presence of substantial amounts of H_2, as well as suitable metal catalysts, appears to be essential in the low-temperature production of abiotic CH_4, as observed in published FTT experiments.

Key words: Fischer–Tropsch reactions, hydrogen, methane, olivine hydration, serpentinization

Received 6 October 2014; accepted 23 September 2015

Corresponding author: Anna Neubeck, Department of Geological Sciences, Stockholm University, Svante Arrhenius väg 8, 10961 Stockholm, Sweden.
Email: anna.neubeck@geo.su.se. Tel: +46 (0)8 16 47 47. Fax: +46 (0)8 674 78 97.

Geofluids (2015)

INTRODUCTION

Hydrous alteration of ultramafic rocks (serpentinization), such as peridotites, has been the focus of numerous studies because of its ability to produce bio-available energy sources, especially methane (CH_4) and hydrogen (H_2). In the presence of trace metals (e.g., Fe, Ni, Co, Zn, Mn), CH_4 and H_2 may play important roles in the origin of life (e.g., Russell *et al.* 2010), may support the deep subsurface biosphere (Nealson *et al.* 2005; McCollom 2007; Hellevang 2008; Klein & Bach 2009), and may be a source of CH_4 on other planets (e.g., Tobie *et al.* 2006; Atreya *et al.* 2007; Etiope *et al.* 2013a). Laboratory experiments demonstrated that the hydration of olivine and pyroxenes, the main minerals in peridotites, can produce H_2 under a wide range of temperatures, from below 100°C (Mayhew *et al.* 2013; Neubeck *et al.* 2014; Okland *et al.* 2014), simulating land-based peridotite systems, to >200°C, such as in hydrothermal conditions similar to those of peridotite-hosted systems in mid-ocean ridges (Shock 1990; Berndt *et al.* 1996; McCollom 2000, 2007; McCollom & Seewald 2001, 2006; Allen & Seyfried 2003; Seewald *et al.* 2006). Abiotic CH_4, frequently observed in serpentinized systems either in the seafloor or on land (see reviews by McCollom 2013; Etiope & Sherwood Lollar 2013; Etiope & Schoell 2014), is considered to typically

stem from Fischer–Tropsch Type (FTT) reactions involving H_2 (generated by peridotite hydration) and a carbon-bearing molecule in the gas phase or in aqueous solution (CO, CO_2, HCO_3^-, CO_3^{2-}). FTT reactions encompass the Fischer–Tropsch reaction *sensu stricto*, involving CO (R1) and the Sabatier reaction involving CO_2 (R2):

$$(2n+1)H_2 + nCO \rightarrow C_nH_{(2n+2)} + nH_2O \quad (R1)$$

$$CO_2 + 4H_2 \rightarrow CH_4 + 2H_2O \quad (R2)$$

Fischer–Tropsch Type reactions need a catalyst, metal or oxides, typically iron, magnetite, chromite, cobalt, or a platinum group element (PGE), for example, ruthenium and rhodium (Foustoukos & Seyfried 2004; Taran *et al.* 2007; Etiope & Ionescu 2014; and references therein). FTT reactions can be detached from the serpentinization reaction because CH_4 production may occur in a rock or fluid–rock interaction system and at temperatures that are different from those that produced H_2. After serpentinization, in fact, H_2 may migrate and accumulate in another rock, far from its serpentinized source rock, and either the new H_2 reservoir rock or the fractured rocks along the H_2 migration pathway can be loci of FTT reactions if CO_2 and the right catalysts are available (Etiope 2015).

An alternative mechanism foresees the possibility that CH_4 is produced right after H_2 in the same serpentinization system, with pre-existing CO_2 during peridotite hydration. This reaction was theoretically proposed by Oze & Sharma (2005):

$$\underset{\text{Olivine}}{24(Mg,Fe)_2SiO_4} + 26H_2O + CO_2 \rightarrow \underset{\text{Serpentine}}{12(Fe)_3Si_2O_5(OH)_4} + \underset{\text{Magnetite}}{4Fe_3O_4} + CH_4 \quad (R3)$$

In this reaction, H_2 can be an intermediary product, but it cannot be excluded that CO_2 is also reduced to CH_4 by Fe(II) or chromian spinel (Oze, personal communication; Foustoukos & Seyfried 2004). In any case, CO_2 participates in the hydration process, and CH_4 production occurs in the same hydration system at the same temperature of serpentinization without initial H_2. The reaction (R3) is thermodynamically favored at low temperatures, below 300°C (Oze & Sharma 2005). This mechanism was considered by Miura *et al.* (2011) to explain CH_4 observed in inclusions of peridotite samples from Oman and by Boschetti *et al.* (2013) and Etiope *et al.* (2013b) as one of several potential processes that could explain the presence of abiotic CH_4 in the absence of H_2 in hyperalkaline waters in Italy and Greece. Reaction (R3) was then proposed by Suda *et al.* (2014) to explain abiotic CH_4 observed in a low-temperature (50–60°C) active serpentinization site in Japan. Suda *et al.* (2014) considered that CH_4 is directly produced from H_2O in the reaction without H_2 mediation. Critiques of this mechanism were raised by Whiticar & Etiope (2014).

The generation of H_2 during olivine hydration is, however, controlled by several factors: temperature, iron content in the olivine, Fe^{2+} partition into secondary minerals, availability of water and pore/fracture space, and silica (SiO_2) activity (Frost & Beard 2007; McCollom & Bach 2009; Katayama *et al.* 2010; Hellevang *et al.* 2011; Klein & McCollom 2013). The role of silica is controversial. For example, Katayama *et al.* (2010) suggest that low amounts of silica are a prerequisite for H_2 production, whereas Klein & McCollom (2013) theoretically predicted H_2 production at high (mM range) silica concentrations. The combination of the several H_2-controlling factors is likely decisive.

In this work, we tested R3 in a laboratory experiment at low temperature (50°C) using natural forsteritic (Mg-rich) dunite and relatively high (mM) concentrations of SiO_2. CO_2 was added as a gas, strictly following the reaction, instead of dissolved carbonate, to avoid the interference with the SiO_2 solution observed in previous experiments (Neubeck *et al.* 2011). Our test was conducted at 50°C to simulate natural, land-based serpentinization sites, typically characterized by low temperatures generally below 100°C (e.g., Boschetti *et al.* 2013; Etiope *et al.* 2013a,b; Morrill *et al.* 2013; Szponar *et al.* 2013; Monnin *et al.* 2014; Suda *et al.* 2014; Etiope 2015). A recent study by Okland *et al.* (2014) shows the experimental abiotic formation of both CH_4 and H_2 through the hydration of powdered dunite at temperatures as low as 25°C. The difference between the study by Okland *et al.* (2014) and the present experiment is both in the grain size and the shaking of the hydrothermal vessel. In this study, we do not use fine-powdered dunite but sand-sized grains, and we do not apply any shaking to the experiments. Okland *et al.* (2014) also used deionized water without the addition of $CO_{2(g)}$.

MATERIALS AND METHODS

Experimental setup

The experiment was designed to investigate the reaction (R3) by mixing forsteritic dunite, dissolved SiO_2, gaseous CO_2, and water at 50°C in borosilicate glass bottles (118 ml). Thirty sample bottles were prepared, containing approximately 10 g of sand (110 ml CO_2 and 30 ml aqueous SiO_2 solution, 1 mM). The same amounts of CO_2 and dissolved SiO_2 were used in 30 control (blank) bottles without dunite. All bottles were stored in a thermostated oven at 50°C. Three samples and three blank bottles were analyzed each time at days 0 and 1 and then at intervals ranging from 20 to 36 days, for a total of ten steps (last samples analyzed after 240 days, i.e., 8 months). After

sampling, the bottles were removed from the experiment. The use of replicates analytically spread the results but decreased the risk of contamination because no bottle was penetrated by a needle or sampled more than once, which decreased the risk of leakage.

The experiments performed in this study were batch experiments without stirring, which prevented the exposure of any fresh mineral surfaces to possible reactants. This setup was chosen to track the fate of SiO_2 in the experiments. Without stirring, it is easier to identify coating on the mineral surfaces.

Materials: bottles, dunite, silica, and CO_2

Before use, the bottles were washed with concentrated HNO_3 (puriss, Sigma-Aldrich) and sterilized at 400°C for 15 h. Black, H_2-tight, NaOH-washed rubber septa (Gotlands Gummifabrik AB, Gotland Rubber Factory Inc., Sweden) were used in all bottles. All bottles were flushed with oxygen-free N_2 (oxygen trap) and vacuum-pumped five times with concomitant sand bath heating (100°C) prior to the addition of the SiO_2 solution to remove adsorbed contaminants. Before injection of 110 ml of CO_2 gas, all flasks were vacuum-pumped for 10 min. Prior to sampling, all samples were sterilized by autoclaving at 120°C for 2 h and cooled to room temperature before incubation at 50°C.

Natural forsteritic dunite (Forsterite 92, Fo92, artificially crushed dunite with a specific surface area of 0.4044 $m^2\ g^{-1}$) was obtained from North Cape Minerals in Åheim, Norway. Contaminants, such as steel fragments (from the crushing of the dunite) and magnetic accessory minerals that could affect the results of the experiments because of their strong reducing capacity, were removed using a Franz magnetic separator. The dunite was cleaned with water (pure Milli-Q) until all of the fine particles (<63 μm) and dust were removed (~15 times). Thereafter, the dunite was cleaned with acetone (Merck, SupraSolv®) in an ultrasonic bath 3 times for 15 min. and dried (100°C) overnight. The forsterite-dominated dunite contained accessory minerals including chlorite, talc, phlogopite, and an Fe-Cr oxide (likely a chromium spinel or chrome-bearing chlorite, see Appendix Fig. A1). Other possible accessory minerals present in the dunite were pyroxenes and magnesite (Neubeck *et al.* 2011). Chopra & Paterson (1984) define the composition of Åheim dunite as 96% olivine, 4% accessory minerals (mainly pyroxene, clinochlore, and phlogopite), and less than 1% spinel (mainly Cr spinel). Microscopic analyses of the dunite show both interstitial spinel crystals and well-defined chlorites (Fig. A1, Appendix). Total bulk elemental concentrations of the initial material are presented in Table A1 (Appendix). The 1 mM aqueous SiO_2 solution was obtained by mixing SiO_2 powder (Sigma-Aldrich) in 18.2 Ω Milli-Q water and heating until dissolved. The CO_2 used for all the experiments was 1% ± 0.02 CO_2, hydrocarbon-free, standard (Air Liquide).

Gas analyses

Methane and CO_2 were analyzed through the injection of 3 ml of headspace gas with a sterile needle into a gas chromatograph (SRI 8610C preconfigured multiple gas analyzer equipped with a methanizer and FID; CH_4 detection limit: 100 ppbv; analytical error: ±5 RSD%).

The stable carbon isotope ratio of CH_4 ($\delta^{13}C_{CH4}$) and CO_2 ($\delta^{13}C_{CO2}$) was measured (UC Davis Stable Isotope Facility, USA) on a Thermo Scientific PreCon concentration system interfaced to a Thermo Scientific Delta V Plus isotope ratio mass spectrometer (IRMS; Thermo Scientific, Bremen, DE). Gas samples were purged from vials through a double-needle sampler into a He carrier stream (20 ml min^{-1}), which was passed through a H_2O/CO_2 scrubber ($Mg(ClO_4)_2$, Ascarite) and a cold trap cooled by liquid nitrogen. The CH_4 was separated from residual gases on an Rt-Q-BOND GC column (30 m × 0.32 mm × 10 μm, 30°C, 1.5 ml min^{-1}). After CH_4 eluted from the separation column, CH_4 was pyrolyzed in an empty alumina tube heated to 1350°C (δ^2H) and subsequently transferred to the IRMS. Laboratory standards were commercially prepared CH_4 gas diluted in helium or air and were calibrated against NIST 8559 (±0.09‰), 8560 (±0.09‰), and 8561 (±0.09‰).

CO_2 was sampled by a six-port rotary valve (Valco, Houston TX) with a 100 μl loop programmed to switch at the maximum CO_2 concentration in the He carrier gas. CO_2 was then separated from N_2O and other residual gases on a Poraplot Q GC column (25 m × 0.32 mm ID, 45°C, 2.5 ml min^{-1}). Two laboratory standards were analyzed between every 10 samples. The laboratory standards were calibrated directly against NIST 8545.

Molecular hydrogen (H_2) was analyzed to track the possible H_2O reduction reaction in which Fe(II) is oxidized and H_2O is reduced to H_2. A headspace sample was transferred by syringe to a sample loop of 500 μl and injected into a gas chromatograph with a reducing compound (HgO bed) photometer (Peak Performer Reduced Gas Analyzer PP1) to measure H_2.

The H_2 was separated from the matrix gas through a system of two packed (a zeolite MS13X 60/80 with a length of 16.5″ and a Unibead silica 1S 60/80 with a length of 81″) columns using N_2 carrier gas. The H_2 was indirectly detected and quantified by the liberated mercury vapor from the heated HgO bed with a UV (254 nm) absorption photometer. A 10 ± 2 ppmv H_2 standard (Air Liquide) was used for calibration.

Thermogravimetric analysis (TGA) coupled to Fourier transform infrared spectrometry (FTIR) was used to measure and quantify gases adsorbed and incorporated in the dunite. The instrument used was a Perkin–Elmer Pyris 1 with an atmosphere of nitrogen and a gas flow of 45 ml min^{-1}. The sample was analyzed between 25 and 1000°C with a ramping rate of 10°C min^{-1} and a Perkin–Elmer FTIR Spectrum 2000.

Liquid- and solid-phase analyses

The dissolved elemental content (Si, Fe, Mg) was measured by removing 5 ml of liquid from the bottles using a sterile needle. The sample was poured into a sterile test tube with 5 µl of pure concentrated HNO_3 (puriss, Sigma-Aldrich) and measured by inductively coupled plasma-optical emission spectroscopy (ICP-OES Spectro, Varian Vista AX) with Ar as the carrier gas. The analytical error was ~4%.

Dissolved inorganic carbon (DIC) was measured on a Shimadzu TOC-Lcph (high-temperature catalytic combustion with NDIR detection of CO_2) to track any formed carbonates.

The pH of the liquid was measured before and after autoclaving, once in the middle of the experiments (after approximately 4 months) and after the experiment termination, using a pHenomenal pH electrode (VWR).

Surface composition and topography were analyzed semi-quantitatively on an XL30 environmental scanning electron microscope (ESEM) with a field emission gun (FEG). The ESEM was equipped with an Oxford X-act energy dispersive spectrometer (EDS), a backscatter electron detector (BSE) and a secondary electron detector (SE). Peak and elemental analyses were made using INCA Suite 4.11 software. None of the samples were coated. The degree of crystallinity and chemical composition of the precipitated material (O2) were studied using a transmission electron microscope (TEM), Jeol 2000FX, equipped with a silicon drift energy dispersive detector, Thermo Scientific NORAN System 7. The sample was distributed on a lacey carbon film supported on a copper grid. Images were recorded both in bright- and dark-field mode to image the amorphous and crystalline material, which was revealed by electron diffraction.

Secondary mineral phases were identified with X-ray diffraction (XRD) using a Siemens D5000 theta/theta diffractometer with CuKα radiation and a graphite monochromator at 40 kV and 40 mA. Peak identification and analyses were made using the software program HighScore Plus 4.0 (PANalytical for X′pert). XRD was conducted on approximately one microgram of precipitates that was smeared onto a sample holder and analyzed conventionally. Unreacted olivine was analyzed in the same manner and withdrawn from the spectra of the precipitate.

RESULTS

Gas phase

The analytical results of the gas composition evolved in the bottle headspace during the 10 steps of incubation are reported in Table 1 as the average of three bottles for each time step. No significant amounts of CH_4 were observed (Fig. 1A, Table 1). Concentrations were always below 1 ppmv, and a one-way ANOVA test showed no statistically significant differences between the group mean values (samples and blanks) with a *P*-value of 0.37. The low CH_4 concentration fluctuated throughout the duration of the experiment around a total average net (sample blank) CH_4 concentration of 0.10 ± 0.15 ppmv, which denotes insignificant CH_4 formation. The TGA analyses of the dunite show that the forsteritic dunite sample weight does not decrease at temperatures below 500°C (Fig. 2). The total weight loss from heating of the dunite at 1000°C was 0.24%, which corresponds to a total gas release of approximately 2.11 ppmv if all dunite were to completely dissolve. The weight gain of approx. 0.02 wt% in beginning of the

Table 1 Concentration of accumulated CH_4, H_2, and CO_2 gas through time in the headspace of the bottles.

Time (days)	Samples (ppmv)	Blanks (ppmv)	Samples blanks (ppmv)
CH_4			
0	0 ± 0	0 ± 0	
1	0.22 ± 0.08	0.16 ± 0.03	0.06 ± 0.05
33	0.29 ± 0.13	0.44 ± 0.43	−0.15 ± 0.28
64	0.61 ± 0.12	0.29 ± 0.05	0.32 ± 0.08
92	0.62 ± 0.31	0.66 ± 0.16	−0.04 ± 0.24
125	0.74 ± 0.13	0.43 ± 0.03	0.32 ± 0.08
155	0.73 ± 0.38	0.53 ± 0.04	0.20 ± 0.21
184	0.68 ± 0.06	0.58 ± 0.16	0.09 ± 0.11
204	0.57 ± 0.12	0.71 ± 0.30	−0.14 ± 0.21
240	0.95 ± 0.35	0.62 ± 0.15	0.34 ± 0.25
H_2			
0	1.88 ± 0.12	1.86 ± 0.35	0.02 ± 0.23
1	4.55 ± 1.45	3.25 ± 1.35	1.30 ± 1.40
33	7.24 ± 0.48	3.88 ± 1.67	3.37 ± 1.08
64	5.61 ± 0.96	3.43 ± 0.01	2.17 ± 0.48
92	8.29 ± 0.59	3.94 ± 0.15	4.36 ± 0.37
125	7.35 ± 0.56	4.21 ± 0.14	3.14 ± 0.35
155	6.20 ± 1.54	3.34 ± 0.20	2.87 ± 0.87
184	7.30 ± 0.51	4.93 ± 0.06	2.37 ± 0.29
204	6.88 ± 0.41	2.41 ± 0.02	4.47 ± 0.22
240	5.36 ± 0.15	3.90 ± 0.01	1.46 ± 0.08
CO_2			
0	1901.40 ± 168.12	2263.32 ± 24.36	−161.93 ± 96.24
1	1251.26 ± 225.92	2304,8 ± 17.23	−1053.54 ± 121.58
33	119.02 ± 47.08	2373.77 ± 19.37	−2254.75 ± 33.23
64	74.77 ± 10.99	2020.89 ± 71.44	−1946.12 ± 41.21
92	93.85 ± 29.48	1861.56 ± 138.74	−1767.70 ± 84.11
125	119.11 ± 14.99	1932.26 ± 126.82	−1813.14 ± 70.90
155	148.39 ± 58.04	1697.05 ± 109.29	−1548. 66 ± 83.67
184	150.01 ± 12.71	1515.05 ± 6.36	−1365.04 ± 9.54
204	125. 46 ± 15.50	570.60 ± 138.34	−1445.14 ± 76.92
240	119.98 ± 31.53	1464.17 ± 235.09	−1344.19 ± 133.31

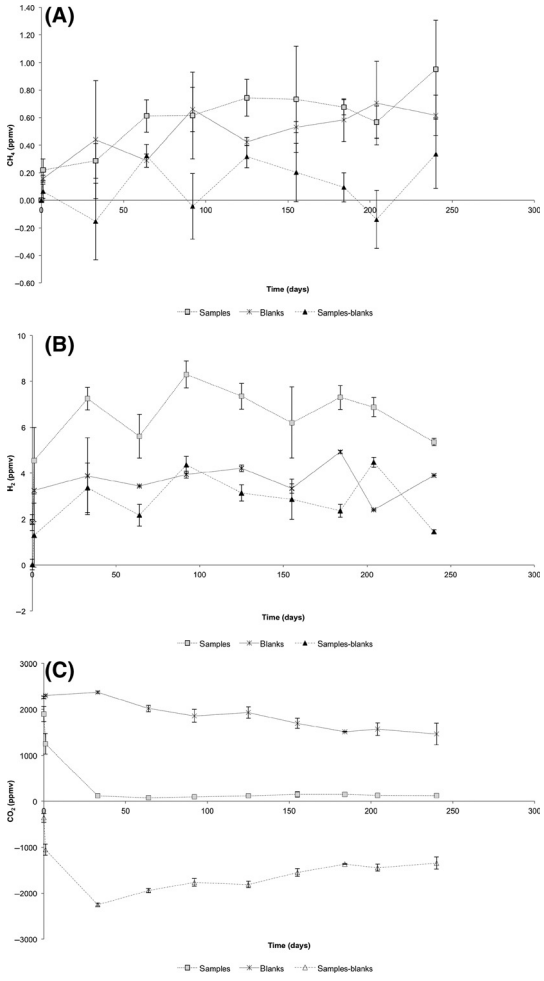

Fig. 1. Concentrations (ppmv) of (A) CH4 (B) H2 and (C) CO2 in the bottle headspace as a function of time.

experiment (Fig. 2) is caused by buoyancy effects, which reduce the density of the surrounding gas in the heating process. Typically, this results in an apparent weight gain of 50–200 μg. Because buoyancy effects are reproducible, the curves were corrected by performing an automatic blank curve subtraction. This also applies to buoyancy effects due to gas switching, which is often used in TGA analysis. The weight loss was calculated from 100% of the total weight, which is the blank corrected value.

Hydrogen accumulated in the incubation bottle headspace and fluctuated around approximately 2.55 ± 1.39 (ppmv, samples blanks) throughout the entire experiment (Fig. 1B, Table 1), which corresponds to a net average H_2 formation of 0.26 ppmv g^{-1} dunite. The highest net concentration of H_2 was 4.47 ppmv on day 204 (Fig. 1B). A general trend of slow H_2 increase was observed. The calculated accumulation rate showed a slight increase in H_2 of 0.012 ppmv day^{-1} (if calculated by comparing day 1 with day 240). However, if the accumulation rate is calculated from a general trendline slope, the net accumulation is only 0.0058 ppmv day^{-1}. The differences between the blanks and the samples in this study are significant when evaluated through an ANOVA test with a *P*-value of 7.4×10^{-4}.

At a constant temperature of 50°C and a pH of 8.2, the concentrations of dissolved CO_2 species were 36.25 μM for H_2CO_3, 2.98 mM for HCO_3^-, and 31.57 μM for CO_3^{2-} after 240 days of incubation. The carbon dioxide concentration (Fig. 1C, Table 1) decreased rapidly after one month in the sample bottles and progressively, but slightly, in the blank bottles. The average net (samples blanks) decrease was -1490.02 ± 75.07 ppmv. The rate of decrease in the blank control bottles was calculated from

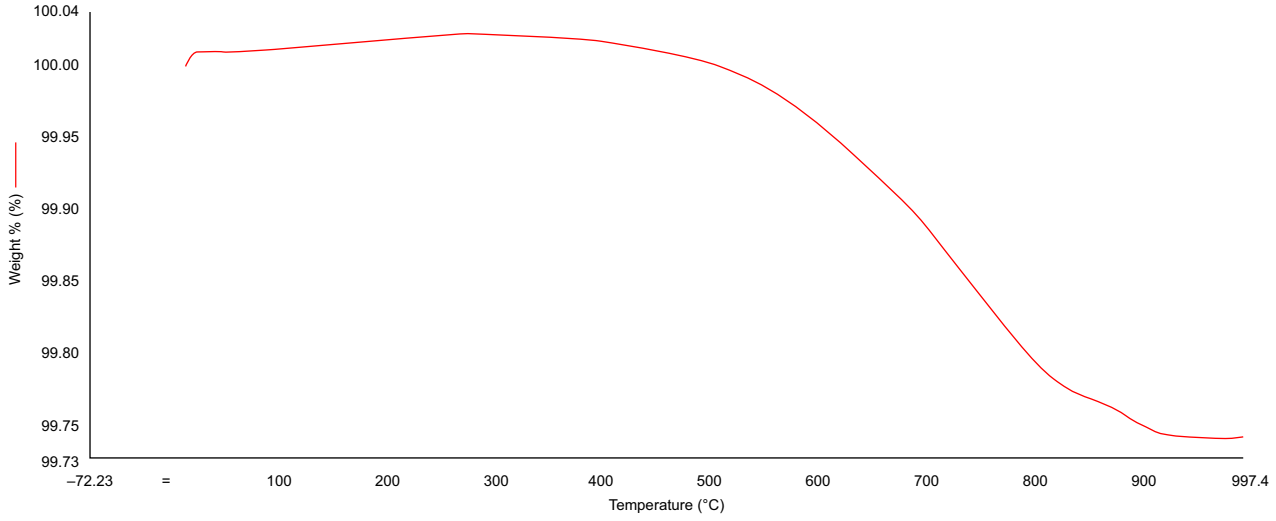

Fig. 2. TGA measurements of olivine showing the released gas in wt% (red line) after heating the sample to 1000°C.

the almost linear trend to be approximately 7.92 ppmv × day^{-1} or 0.79 ppmv × day^{-1} × g $dunite^{-1}$. The greater decrease in CO_2 in the bottles with added dunite can be explained by a higher concentration of cations in the solution, providing reactants for the anionic carbon species. However, because the saturation of carbonate was not reached, no observable precipitates of metal carbonates could be found.

No significant differences between the blank and sample $\delta^{13}C$ values were observed in either the CH_4 or CO_2 measurements (Table 2). The error bars among the three replicates overlap the sampled values, making any difference between the measured samples nonsignificant. The isotopic analyses of the CO_2 and CH_4 in the experiments in this study show that the accumulation of CH_4 was not produced by dunite hydration because all blanks and samples had the same isotopic composition.

Aqueous and solid phase

In the present study, dissolved SiO_2 was added to the solution prior to CO_2, which resulted in the amorphous SiO_2-rich precipitate covering on the dunite surface (Fig. 3, TEM and ESEM analyses). Precipitates were observed both in solution and on the dunite grains where they covered large parts of the grain surfaces (Fig. 3). The precipitate was composed of SiO_2 with Mg in all of the samples and Fe in some of the samples. The precipitates had an Mg+Fe/Si molar ratio ranging between 0.87 and 1.7, which covers the Mg + Fe/Si ratio of serpentine (1–1.5, calculated from the generic formula for serpentine). The Mg/Si mass ratio of the precipitates found in the solution was 0.12 (calculated from the TEM analyses, Table 2), which is different from the initial dunite Mg/Si ratio (1.8, calculated from the generic formula of Fo92).

Bulk samples of precipitates measured by XRD and Raman showed no identifiable phases likely due to the poor crystallinity of the precipitated material. Due to the heterogeneous character of the precipitate, not much information could be extracted from the XRD measurements. The precipitates formed were, according to the TEM analyses, all amorphous silicates with trace metal contents varying between 0 and 20 at% (atomic %), see Fig. 3. The detection of carbonates was ambiguous. Some analyses showed the presence of carbonates and some did not. Acid treatment of the dried precipitates showed clear bubbling, indicating the formation of carbonates. However, because of the ambiguousness, the influence of the carbonates on the dissolution of dunite could not be determined. The DIC concentration of the solution was 23.67 mg l^{-1}.

Elemental release into solution was analyzed to trace possible precipitation events (all elemental ICP-OES data is presented in Appendix, Table A2). Because Mg, Si, and Fe were the major elements found in the precipitates, these elements were also analyzed in solution. The amount of Si varied incongruently with both the amount of Fe and Mg in solution (Fig. 4A–B), whereas Fe and Mg varied congruently (Fig. 4B–C). A slight decrease in the concentration of Si can be observed with time, which is expected due to the precipitation of SiO_2 on the olivine surface and within the solution. The rate of increased concentration of Fe was calculated as 0.047 ppm day^{-1}.

The pH was initially 5.8 ± 0.1 (before autoclaving and including 1 mM Si, CO_2 and dunite) and then 6.5 ± 0.2 directly after autoclaving. In the blanks, the pH was initially the same as the sample bottles. The pH was then measured on day 33 and after termination of the experiment and had a relatively constant value of 8.2 ± 0.2 throughout the rest of the experiment.

DISCUSSION

Our laboratory test of the reaction (R3) did not produce significant amounts of CH_4. The presence of CH_4 in the

Table 2 Stable carbon isotope values ($\delta^{13}C$ ‰, VPDB) of CO_2 and CH_4 in the headspace of the incubation bottles. The concentration (ppmv) here reported refers to the sample glass vials measured by UC Davis Stable Isotope Facility and may therefore differ from the measured concentrations in the samples in Table 1.

Days of incubation	Blank samples	Concentration (ppmv)	Olivine samples	Concentration (ppmv)	Compound
Initial value	−25.01	2308	−25.01	22895	CO_2
0	−24.96	2297	−26.77	1270	CO_2
0	−24.92	2078	−27.01	1326	CO_2
0	−24.92	2329	−27.33	1223	CO_2
98	−24.84	806	−22.64	49	CO_2
98	−25.41	640	−25.09	53	CO_2
98			−27.41	51	CO_2
240	−26.23	924	−25.46	148	CO_2
240	−24.08	1117	−28.76	177	CO_2
240	−23.62	1107	−25.64	170	CO_2
240	−49.47	0.30	−48.25	0.50	CH_4
240	−50.21	0.20	−51.09	0.40	CH_4
240	−50.55	0.30	−49.39	0.30	CH_4

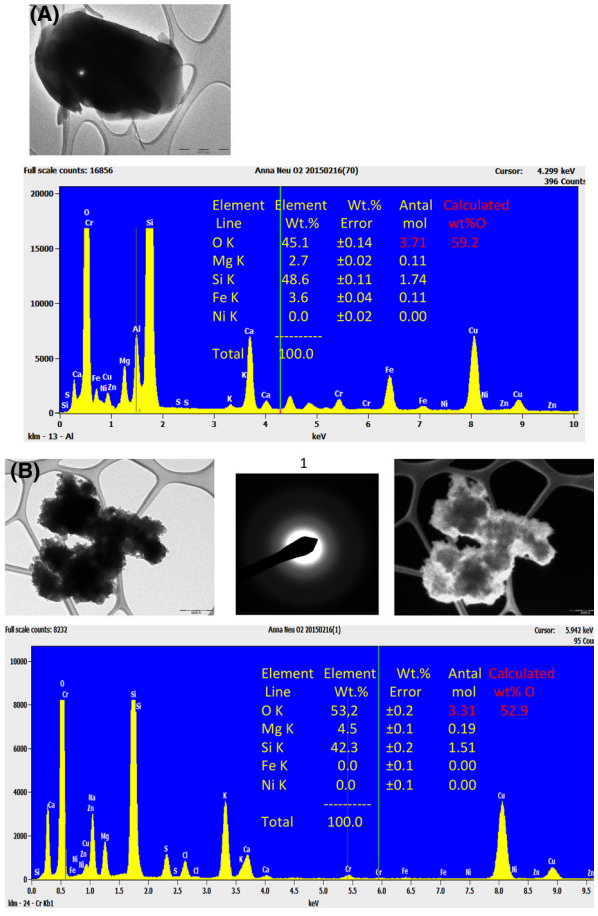

Fig. 3. ESEM image (A) showing the precipitates (white) that covered the olivine surfaces (gray), (B) showing the elemental composition of the precipitates within the solution measured with ESEM, and (C) showing the elemental composition of the precipitates within the solution measured with TEM.

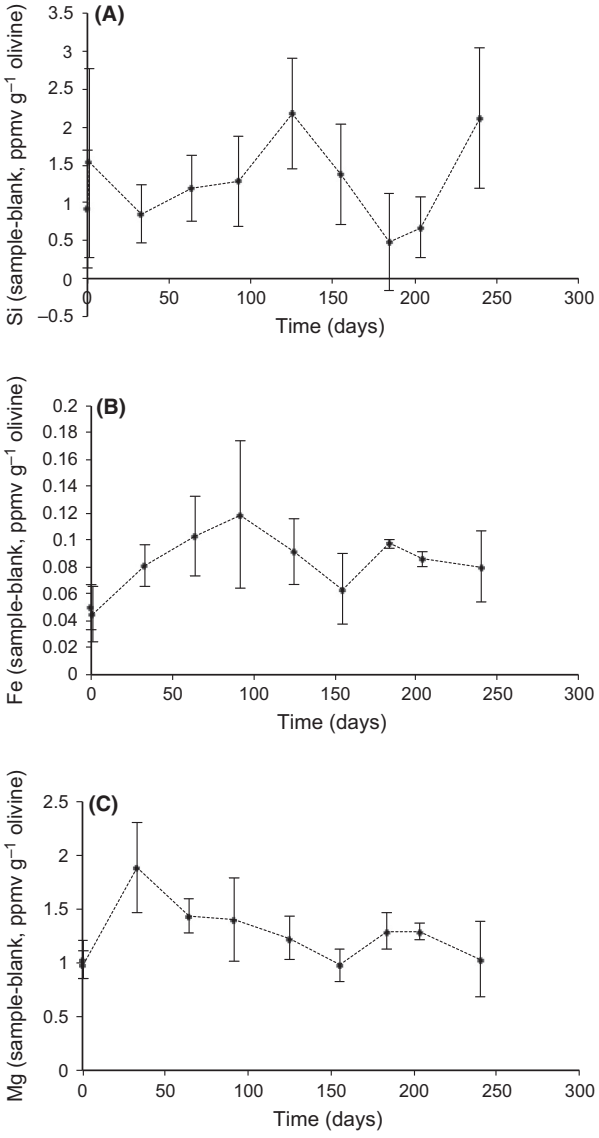

Fig. 4. Net variation of (A) Si, (B) Fe, and (C) Mg in solution (mg L^{-1} g olivine^{-1}) as a function of time.

blanks could be explained by a possible release of CH_4 from the rubber septa and not from incorporation of CH_4 in the dunite mineral because there were no significant differences between the concentration of CH_4 in the samples and in the blanks. Leakage from the rubber septa was tested, and no leakages of CH_4, CO_2 or H_2 could be observed. However, because the GC detection limit is 0.1 ppmv and the analytical error is 5 RSD% (relative standard deviation), the measured CH_4 could also be considered analytical noise. Although all rubber septa were boiled in concentrated NaOH prior to use and leakage was not detected when analyzed, minimal long-term leakage from the septa cannot be ruled out. The lack of CH_4 formation within the conditions of this experiment is likely due to the scarce redox potential of the system and insufficient generation of H_2. In our experiment, the production of H_2 was very low and likely not enough to have an effect on the reduction of CO_2. The Sabatier reaction (R2), which can be an intermediary step in (R3), requires an H_2:CO_2 ratio of at least 4:1 and a metal catalyst suitable for the temperature of the experiment. The 4:1 ratio was not attained in our experiment, and the available catalyst, basically Fe, was likely unable to support the low-temperature FTT reactions, as observed in previous works (Etiope & Ionescu 2014). If (R3) can proceed without mediation of H_2 (i.e., without intermediary reaction R2), as hypothesized by Suda *et al.* (2014), other carbon reducing factors should be considered.

In our experiment, the H_2 production rate was an order of magnitude lower than that reported by Neubeck *et al.* (2014), which had an average net H_2 production of 39.87 ± 13.20 ppmv in the presence of dissolved Na_2CO_3. The temperature and SiO_2 concentration were

comparable in both experiments, but in Neubeck *et al.* (2014), 20 mM of Na_2CO_3 was also added to the solution. In our study, no Na_2CO_3 was used, but CO_2 (g) was added to the headspace of the bottles instead as a reactant for possible CH_4 formation through a slow diffusion into the aqueous solution (resulting in a slightly lower pH) and reaction with dunite. Therefore, SiO_2 could possibly act without the influence of HCO_3^- at the beginning of the experiment and thus possibly hinder the formation of H_2 through precipitation onto the olivine surface as a coating barrier against further dissolution. The ceased dissolution of olivine is supported by the observation of a SiO_2-rich coating on the olivine surface (Fig. 3) and the decreased release of Mg and Fe into solution with time (Fig. 4). Our interpretation of these results is that SiO_2 in this study, in comparison with the work in Neubeck *et al.* (2014), hindered H_2 formation even at temperatures as low as 50°C and at concentrations of 1 mM due to SiO_2 coating. In Neubeck *et al.* (2011), a similar pattern was observed, namely that the experiments with added carbonates to the solution increased the amount of H_2 in the experiments. Stevens & McKinley (2000) showed that H_2 production (from basalts) increased with increasing acidity between 30 and 60°C: pH 9 resulted in the lowest production of H_2, and pH 8 had a higher production. In Klein & McCollom (2013; using Fo90) as well as in Neubeck *et al.* (2011, 2014) and this study, using forsteritic dunite), we see an opposite trend, in which H_2 production was higher with increasing pH from ~8 to ~9 potentially due to a decreased reactivity of SiO_2 at higher pH and/or an increased ability of Fe(II) to become oxidized into Fe(III) at a higher pH. The differences in H_2 production between this study and Stevens & McKinley (2000) are likely due to the difference in minerals used in the experiments.

In the experiment with added HCO_3^-, the H_2 production was consistently higher (Neubeck *et al.* 2011, 2014) as long as the system remained undersaturated with respect to carbonates. Jones *et al.* (2010) showed that the production of H_2 proceeds more rapidly in an undersaturated carbonate system than in a saturated carbonate system and when small amounts of carbonates are added.

The higher H_2 formation in Neubeck *et al.* (2014) is likely due to the coprecipitation of SiO_2 and CO_3^{2-} (Kellermeier *et al.* 2010, 2012a,b). Coprecipitation of SiO_2 and CO_3^{2-} causes a withdrawal of net SiO_2 from the solution (removing SiO_2 that otherwise would precipitate onto the olivine surface as a thin film), allowing for continued dunite dissolution and H_2 formation. In the present study, dissolved SiO_2 was added to the solution prior to CO_2, which resulted in the amorphous SiO_2-rich precipitate observed covering the dunite surface (Fig. 3, TEM and ESEM analyses), lowering the rate of dunite dissolution and the production of H_2 (Mayhew *et al.* 2013). At pH <9, SiO_2 is also more prone to condensation due to a higher degree of protonation, which will increase the rate of SiO_2 precipitation (Kellermeier *et al.* 2012a,b). A lower pH and a lower net concentration of dissolved CO_3^{2-} in this study, compared with Neubeck *et al.* (2014), would lower the degree of precipitation of carbonates as well as the withdrawal of SiO_2 from the solution.

The ratio of average error to average sample concentration of H_2 was 1.15 in this study compared to 0.15 in Neubeck *et al.* (2014). This means that the spread of the measured points was larger in this experiment, most likely due to the lower measured concentrations of H_2.

The release of Fe and Mg is due to the dissolution of olivine and is therefore expected to have similar concentration patterns with time, and the fluctuating patterns of increased and decreased concentrations could be due to a buildup of ions in solution until a threshold concentration is reached and the precipitation forms. When the precipitate forms, the concentration of ions in solution also decreases and another round of concentration buildup begins. If this was the case here, one would expect the threshold level to rise slightly as the Si concentration decreases, which can also be seen in the plots in Fig. 4A–C. The average rate of increasing Fe concentration was calculated as 0.047 ppm day^{-1}, which is 4 times that of the H_2 accumulation rate, meaning that there was enough Fe released into solution to support a reduction of H_2O into H_2. Comparisons between $H_{2(g)}$ and $Fe_{(aq)}$ fluctuations over time show that H_2 and Fe generally coincide (Figs 1 and 4B and Fig. A2 in the Appendix). This general trend of covariation may be indicative of a process in which H_2 is formed through the oxidation and precipitation of Fe (III).

In contrast to what was observed in Neubeck *et al.* (2014), we could not identify any crystalline mineral phases in this study and thus could not assign any formation pathway for the produced H_2 in the bottles. However, the amount of dissolved Fe (for reduction of water) does not seem to have been enough (Fig. 4B) to form H_2 in amounts comparable to those in Neubeck *et al.* (2014). A possible explanation is that Fe^{2+} is deactivated to a greater extent by the precipitation of SiO_2 covering the dunite surface. The Mg+Fe/Si ratios of the precipitates described in the Results section indicate that the precipitation in solution is depleted in Fe compared with the precipitates on the dunite surface. Although the Mg+Fe/Si ratios of the precipitates (0.87–1.7) are close to the ratio of serpentine (1.5), we were not able to identify any serpentine phase with Raman or XRD, likely due to the amorphous and intermediate character of the precipitate.

However, Mayhew *et al.* (2013) described a pathway for H_2 formation through the oxidation of Fe^{2+} promoted by spinels. This scenario could also be possible in our experiment because the dunite had accessory spinels (Appendix,

Fig. A1). Solid phases other than magnetite, such as serpentine, can also possibly incorporate Fe (Evans 2008; Klein *et al.* 2009; McCollom & Bach 2009; Andreani *et al.* 2013).

Pure water with a temperature of 50°C will spontaneously form H^+ ions at pH 6.63 ($Kw = 5.476*10^{-14}$), which will react with any available anions in the solution, such as OH^-, HCO_3^{2-} or SiO_4^{4-}. At pH 6, the polymerization of SiO_2 is rapid and increases with the increasing ionic strength of the solution and with increasing pH up to pH 9.3, when the polymerization rate decreases again (Tarutani 1989). Because of the rapid polymerization of SiO_2 with a low point zero charge (PZC) of 2.0 (Elimelech *et al.* 1995), the metal ions likely have a preferential adsorption/incorporation onto the SiO_2 surface rather than on any carbonate (PZC between 9.40 and 9.70, (Jaafar *et al.* 2013), which is in agreement with our results in which all precipitates contained the major metal ions of the analyzed dunite together with SiO_2. In addition, at the beginning of the experiment, the pH of the solution was below the PZC of any possible precipitated carbonates, which will make the carbonate surface positively charged and thus repel any metal ions. Therefore, the most likely fate of the dissolved Fe(II) was adsorption or precipitation with SiO_2 and not with carbonates. The carbonates found together with the SiO_2 precipitates in Neubeck *et al.* 2014 most likely precipitated when the pH increased to approx. 9. In the present experiments, the amount of dissolved carbon species in solution was undersaturated with respect to carbonates, even though the pH rose slightly above 8. Therefore, nothing can be concluded about any possible precipitation of Fe-bearing carbonates.

In summary, our laboratory test of the reaction (R3), considered by Suda *et al.* (2014) as an important mechanism for abiotic CH_4 generation in land-based serpentinization systems, (i) did not produce any significant amounts of CH_4 in our experimental conditions, (ii) potentially due to the scarce production of H_2 or to a scarce reducing potential in general, (iii) in turn caused by a combination of H_2-inhibiting factors likely including silica activity. These results should be taken into account when interpreting of the origin of abiotic CH_4 after serpentinization in natural conditions.

CONCLUSIONS AND FUTURE STUDIES

Understanding the mechanisms and conditions of abiotic CH_4 and H_2 generation in low-temperature serpentinization systems is fundamental to several research fields, including microbiology of deep rocks and the origin of life on Earth and on other planets. FTT reactions (R1–R2) with abundant H_2 were able to generate considerable amounts of CH_4 even at room temperature (Etiope & Ionescu 2014 and references therein). In geological environments, FTT reactions can be spatially and temporally detached from serpentinization because CH_4 production may occur in a fluid–rock system that is different from that generating H_2. Direct mineral (olivine) hydration assisted by CO_2 in the absence of initial H_2 (R3), proposed by Oze & Sharma (2005), was considered an alternative mechanism, whereby CH_4 is produced in the same serpentinization and H_2-generation system (Suda *et al.* 2014). We tested the reaction (R3). Our experiment conducted with dunite at low temperature (50°C) did not show appreciable CH_4 production. Trace amounts of CH_4 (<1 ppmv) were within the analytical error range and were not significantly different from the control samples (in the absence of dunite). The trace amount of CH_4 can be explained by either a long-term leakage from the rubber septa and/or analytical noise of the GC. Several factors could explain why CO_2 was not reduced to CH_4. First involves the scarce production of H_2 and the lack of suitable metal catalysts in the dunite, both necessary to form CH_4 via FTT reactions. Then, assuming the hypothesis of Suda *et al.* (2014) by which CH_4 could derive from H_2O and not from H_2, there may have been a lack of sufficiently reducing conditions, even though Fe and spinels were present in the system. Either the SiO_2 coated the dunite surface and therefore decreased the amount of reactive surfaces, and/or the ferric iron was consumed by SiO_2 and therefore hindered from reacting as a reducing agent.

Small amounts of abiotic H_2 were observed in the experiments, even though the concentrations were very low. However, added SiO_2 in the mM range did hinder H_2 production, even at the low temperatures used in the experiment. H_2 may have been formed both through the oxidation of Fe^{2+} in solution and through the precipitation of secondary minerals on the surface of the dunite. The reaction products could not be fully established, and therefore, the reaction pathway remains unknown.

Thus far, only FTT reactions have been shown to produce considerable quantities of CH_4, both at high temperatures (>200°C; McCollom 2013; and references therein) and low temperatures (<100°C; Etiope & Ionescu 2014). CH_4 production by low-temperature olivine hydration in the absence of initial H_2 appeared to be sluggish and effective only after special sample treatment (Okland *et al.* 2014).

Future studies on the abiotic reduction of CO_2 through dunite hydration (reaction R3) should extend to longer incubation times (>1–2 years) and should be conducted at higher temperatures (>50°C), at higher CO_2 concentrations and/or with smaller dunite grain sizes. The use of synthesized olivine instead of natural dunite material will also increase the accuracy and control of the measurements, even though such an experiment will be more difficult to translate to natural systems. The role played in

reaction R3 by metal catalysts that are effective for low-temperature FTT reactions (e.g., ruthenium; Etiope & Ionescu 2014) should also be evaluated.

ACKNOWLEDGEMENTS

This work was funded by Petrobras, with coordination of the Istituto Nazionale di Geofisica e Vulcanogia, Rome (project 'Low temperature methanation in geologic environments', contract no. 0050.0073814.12.2). We would like to thank Christian Mille at the Royal Institute of Technology, Sweden, for help with TGA-IR experiments, Heike Siegmund at the Stockholm University Delta Facility for help with the stable isotopic determination and Kjell Jansson at the Electron Microscopy Center in the Department of Materials and Environmental Chemistry, Stockholm University for help with the TEM analysis.

REFERENCES

Allen DE, Seyfried WE Jr (2003) Compositional controls on vent fluids from ultramafic-hosted hydrothermal systems at mid-ocean ridges: an experimental study at 400°C, 500 bars. *Geochimica et Cosmochimica Acta*, **67**, 1531–42.

Andreani M, Daniel I, Pollet-Villard M (2013) Aluminum speeds up the hydrothermal alteration of olivine. *American Mineralogist*, **98**, 1738–44.

Atreya SK, Mahaffy PR, Wong A-S (2007) Methane and related trace species on Mars: origin, loss, implications for life, and habitability. *Planetary and Space Science*, **55**, 358–69.

Berndt ME, Allen DE, Seyfried WE (1996) Reduction of CO_2 during serpentinization of olivine at 300°C and 500 bar. *Geology*, **24**, 351–4.

Boschetti T, Etiope G, Toscani L (2013) Abiotic methane in hyperalkaline springs of Genova, Italy. *Procedia Earth and Planetary Science*, **7**, 248–51.

Chopra PN, Paterson MS (1984) The experimental deformation of dunite. *Tectonophysics*, **78**, 453–73.

Elimelech M, Gregory J, Jia X, Williams RA (1995) *Particle Deposition & Aggregation Measurement, Modelling and Simulation*. Butterworth-Heinemann, Woburn, MA.

Etiope G (2015). *Natural Gas Seepage. The Earth's Hydrocarbon Degassing*. Springer, pp. 199. ISBN 978-3-319-14601-0.

Etiope G, Ionescu A (2014) Low-temperature catalytic CO_2 hydrogenation with geological quantities of ruthenium: a possible abiotic CH_4 source in chromitite-rich serpentinized rocks. *Geofluids*, **15**, 438–52.

Etiope G, Schoell M (2014) Abiotic gas: atypical, but not rare. *Elements*, **10**, 291–6.

Etiope G, Sherwood Lollar B (2013) Abiotic methane on Earth. *Reviews of Geophysics*, **51**, 276–99.

Etiope G, Ehlmann BL, Schoell M (2013a) Low temperature and production of methane from serpentinized rocks on Earth: a potential analog for methane production on Mars. *Icarus*, **224**, 275–85.

Etiope G, Tsikouras B, Kordella S, Ifandi E, Christodoulou D, Papatheodorou G (2013b) Methane flux and origin in the Othrys ophiolite hyperalkaline springs, Greece. *Chemical Geology*, **347**, 161–74.

Evans BW (2008) Control of the products of serpentinization by the Fe^{2+} Mg^{-1} exchange potential of olivine and orthopyroxene. *Journal of Petrology*, **49**, 1873–87.

Foustoukos DI, Seyfried WE (2004) Hydrocarbons in hydrothermal vent fluids: the role of chromium-bearing catalysts. *Science*, **304**, 1002–5.

Frost BR, Beard JS (2007) On silica activity and serpentinization. *Journal of Petrology*, **48**, 1351–68.

Hellevang H (2008) On the forcing mechanism for the H_2-driven deep biosphere. *International Journal of Astrobiology*, **7**, 157–67.

Hellevang H, Huang S, Thorseth IH (2011) The potential for low-temperature abiotic hydrogen generation and a hydrogen-driven deep biosphere. *Astrobiology*, **11**, 711–24.

Jaafar MZ, Nasir AM, Hamid MF (2013) Point of zero charge for sandstone and carbonate rocks by streaming potential. *International Journal of Petroleum & Geoscience Engineering*, **1**, 82–90.

Jones C, Rosenbauer R, Goldsmith JI, Oze C (2010) Carbonate control of H2 and CH4 production in serpentinization systems at elevated P–Ts. *Geophysical Research Letters*, **37**, L14306.

Katayama I, Kurosaki I, Hirauchi K-I (2010) Low silica activity for hydrogen generation during serpentinization: an example of natural serpentinites in the Mineoka ophiolite complex, central Japan. *Earth and Planetary Science Letters*, **298**, 199–204.

Kellermeier M, Melero-Gracia E, Glaab F, Klein R, Drechsler M, Rachel R, Garcia-Ruiz JM, Kunz W (2010) Stabilization of amorphous calcium carbonate in inorganic silica-rich environments. *Journal of the American Chemical Society*, **132**, 17859–66.

Kellermeier M, Melero-Garcia E, Glaab F, Eiblmeier J, Kienle L, Rachel R, Kunz W, Garcia-Ruiz JM (2012a) Growth behavior and kinetics of self-assembled silica-carbonate biomorphs. *Chemistry - A European Journal*, **18**, 2272–82.

Kellermeier M, Melero-Garcia E, Kunz W, Garcia-Ruiz JM (2012b) Local autocatalytic co-precipitation phenomena in self-assembled silica–carbonate materials. *Journal of Colloid and Interface Science*, **380**, 1–7.

Klein F, Bach W (2009) Fe–Ni–Co–O–S phase relations in peridotite-seawater interactions. *Journal of Petrology*, **50**, 37–59.

Klein F, McCollom T (2013) From serpentinization to carbonation: new insights from a CO_2 injection experiment. *Earth and Planetary Science Letters*, **379**, 137–45.

Klein F, Bach W, Jöns N, McCollom T, Moskowitz B, Berquó T (2009) Iron partitioning and hydrogen generation during serpentinization of abyssal peridotites from 15°N on the Mid-Atlantic Ridge. *Geochimica et Cosmochimica Acta*, **73**, 6868–93.

Mayhew LE, Ellison ET, McCollom TM, Trainor TP, Templeton AS (2013) Hydrogen generation from low-temperature water–rock reactions. *Nature Geoscience*, **6**, 478–84.

McCollom TM (2000) Geochemical constraints on primary productivity in submarine hydrothermal vent plumes. *Deep Sea Research Part I: Oceanographic Research Papers*, **47**, 85–101.

McCollom TM (2007) Geochemical constraints on sources of metabolic energy for chemolithoautotrophy in ultramafic-hosted deep-sea hydrothermal systems. *Astrobiology*, **7**, 933–50.

McCollom TM (2013) Miller-Urey and beyond: what have we learned about prebiotic organic synthesis reactions in the past 60 years? *Annual Review of Earth and Planetary Sciences*, **41**, 207–29.

McCollom TM, Bach W (2009) Thermodynamic constraints on hydrogen generation during serpentinization of ultramafic rocks. *Geochimica et Cosmochimica Acta*, **73**, 856–8875.

McCollom TM, Seewald JS (2001) A reassessment of the potential for reduction of dissolved CO_2 to hydrocarbons during serpentinization of olivine. *Geochimica et Cosmochimica Acta*, **65**, 3769–78.

McCollom TM, Seewald JS (2006) Carbon isotope composition of organic compounds produced by abiotic synthesis under hydrothermal conditions. *Earth and Planetary Science Letters*, **243**, 74–84.

Miura M, Arai S, Mizukami T (2011) Raman spectroscopy of hydrous inclusions in olivine and orthopyroxene in ophiolitic harzburgite: implications for elementary processes in serpentinization. *Journal of Mineralogical and Petrological Sciences*, **106**, 91–6.

Monnin C, Chavagnac V, Boulart C, Ménez B, Gérard M, Gérard E, Quéméneur M, Erauso G, Postec A, Guentas-Dombrowski L, Payri C, Pelletier B (2014) The low temperature hyperalkaline hydrothermal system of the Prony bay (New Caledonia). *Biogeosciences Discuss*, **11**, 6221–67.

Morrill PL, Kuenen JG, Johnson OJ, Suzuki S, Rietze A, Sessions AL, Fogel ML, Nealson KH (2013) Geochemistry and geobiology of a present-day serpentinization site in California: the Cedars. *Geochimica et Cosmochimica Acta*, **109**, 222–40.

Nealson KH, Inagaki F, Takai K (2005) Hydrogen-driven subsurface lithoautotrophic microbial ecosystems (SLiMEs): do they exist and why should we care? *Trends in Microbiology*, **13**, 405–10.

Neubeck A, Nguyen Thanh D, Bastviken D, Crill P, Holm NG (2011) Formation of H_2 and CH_4 by weathering of olivine at temperatures between 30 and 70°C. *Geochemical Transactions*, **12**, 6–16.

Neubeck A, Nguyen Thanh D, Hellevang H, Oze C, Bastviken D, Bacsik Z, Holm N (2014) Olivine alteration and H_2 production in carbonate-rich, low temperature aqueous environments. *Planetary and Space Science*, **96**, 51–61.

Okland I, Huang S, Thorseth IH, Pedersen RB (2014) Formation of H_2, CH_4 and N-species during low-temperature experimental alteration of ultramafic rocks. *Chemical Geology*, **387**, 22–34.

Oze C, Sharma M (2005) Have olivine, will gas: serpentinization and the abiogenic production of methane on Mars. *Geophysical Research Letters*, **32**, L10203–7.

Russell MJ, Hall AJ, Martin W (2010) Serpentinization and its contribution to the energy for the emergence of life. *Geobiology*, **8**, 355–71.

Seewald JS, Zolotov MY, McCollom T (2006) Experimental investigation of single carbon compounds under hydrothermal conditions. *Geochimica et Cosmochimica Acta*, **70**, 446–60.

Shock EL (1990) Geochemical constraints on the origin of organic compounds in hydrothermal systems. *Origins of Life and Evolution of the Biosphere*, **20**, 331–67.

Stevens TO, McKinley JP (2000) Abiotic controls on H_2 production from basalt-water reactions and implications for aquifer biogeochemistry. *Environmental Science and Technology*, **34**, 826–31.

Suda K, Ueno Y, Yoshizaki M, Nakamura H, Kurokawa K, Nishiyama E, Yoshino K, Hongoh Y, Kawachi K, Omori S, Yamada K, Yoshida N, Maruyama S (2014) Origin of methane in serpentinite-hosted hydrothermal systems: the CH_4–H_2–H_2O hydrogen isotope systematics of the Hakuba Happo hot spring. *Earth and Planetary Science Letters*, **386**, 112–25.

Szponar N, Brazelton WJ, Schrenk MO, Bower DM, Steele A, Morrill PL (2013) Geochemistry of a continental site of serpentinization, the Tablelands Ophiolite. *Gros Morne National Park: A Mars analogue, Icarus*, **224**, 286–96.

Taran YA, Kliger GA, Sevastianov VS (2007) Carbon isotope effects in the open-system Fischer–Tropsch synthesis. *Geochimica et Cosmochimica Acta*, **71**, 4474–87.

Tarutani T (1989) Polymerization of silicic acid. *Analytical Sciences*, **5**, 245–52.

Tobie G, Lunine JI, Sotin C (2006) Episodic outgassing as the origin of atmospheric methane on Titan. *Nature Letters*, **440**, 61–4.

Whiticar MJ, Etiope G (2014) Hydrogen isotope fractionation in land-based serpentinization systems. Comment on "Origin of methane in serpentinite-hosted hydrothermal systems: the CH_4–H_2–H_2O hydrogen isotope systematics of the Hakuba Happo hot spring" by Suda *et al.* (2014) [*Earth and Planetary Science Letters*, **386**, 112–25]. *Earth and Planetary Science Letters*, **401**, 373–5.

APPENDIX

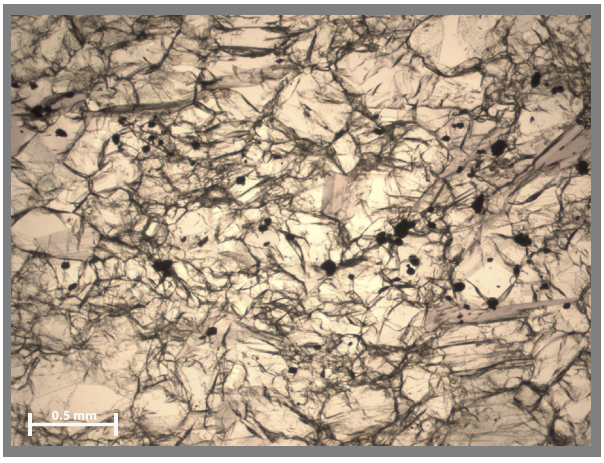

Fig. A1. Optical microscopy image showing an area of the dunite with inclusions of spinels.

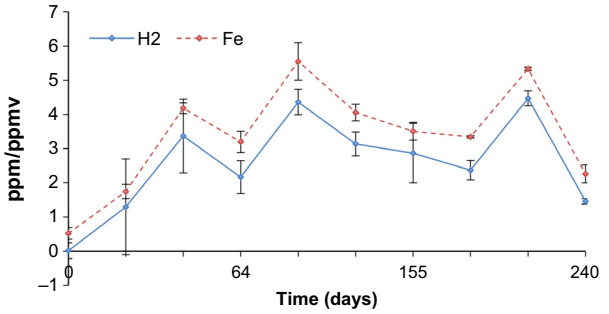

Fig. A2. Variation of H_2 and Fe (samples minus blanks) as a function of time (days), where H_2 is presented in ppmv and Fe in ppm. All data are presented as the average values of three replicates per sample point.

Table A1 ICP-OES bulk analysis of the total elements of dunite. Analysis of As, Cd, Cu, Co, Hg, Ni, Pb, Sb, S, Se, and Zn has been made so that the sample has been dried to 50°C followed by a dry weight correction to 105°C. Dissolution has been made according to the standard method ASTM D3683 (modified). All other elements have been analyzed according to ASTM D3682 ($LiBO_2$-melt).

Compound	Results	Error	Unit	Element	Results	Error	Unit	Element	Results	Error	Unit
SiO_2	41.2	3.3	%	As	<3		mg kg^{-1}	Ni	3010	733	mg kg^{-1}
Al_2O_3	0.213	0.019	%	Ba	<2		mg kg^{-1}	Pb	4.28	1.79	mg kg^{-1}
CaO	<0.09		%	Be	<0.6		mg kg^{-1}	S*	116		mg kg^{-1}
Fe_2O_3	9.03	0.72	%	Cd	<0.1		mg kg^{-1}	Sc	3.34	1.35	mg kg^{-1}
K_2O	<0.1		%	Co	116	26	mg kg^{-1}	Sn*	2.12		mg kg^{-1}
MgO	52.1	4.1	%	Cr	1620	217	mg kg^{-1}	Sr	9.39	1.13	mg kg^{-1}
MnO	0.111	0.011	%	Cu	21.9	4.9	mg kg^{-1}	V	11.4	4.4	mg kg^{-1}
Na_2O	<0.06		%	Hg	<0.01		mg kg^{-1}	W	<60		mg kg^{-1}
P_2O_5	<0.01		%	Mo	71.2	12.8	mg kg^{-1}	Zn*	48.8	10.5	mg kg^{-1}
TiO_2	0.0027	0.0002	%	Nb	<6		mg kg^{-1}	Zr	<2		mg kg^{-1}
Sum	102.7										

Asterisks means that the elemental analyses have been a nonaccredited analysis. Measuring errors is reported as an expanded insecurity according to the definition mentioned in the 'Guide to the expression of uncertainty in measurement' (ISO:IEC Guide 98-3:2008).

Table A2 Raw data from the ICP-OES analyses showing the total amount of elements in solution in samples and blanks.

	Samples					
Days of incubation	Fe	Fe average	Mg	Mg average	Si	Si average
0	447.40		11320.00		9724.00	
0	374.50	171.72	8299.00	1798.39	22670.00	7849.64
0	701.60	507.83	11500.00	10373.00	8506.00	13633.33
1	339.60		8962.00		33670.00	
1	691.60	207.05	11330.00	1314.24	21950.00	12501.48
1	326.70	452.63	9158.00	9816.67	8683.00	21434.33
33	937.50		23470.00		14200.00	
33	876.40	158.76	18130.00	4233.31	20230.00	3778.61
33	637.10	817.00	15110.00	18903.33	13270.00	15900.00
64	961.30		15110.00		15540.00	
64	1388.00	299.94	15470.00	1569.20	19150.00	4334.16
64	809.50	1052.93	12590.00	14390.00	24170.00	19620.00
92	1685.00		17540.00		26360.00	
92	604.90	548.90	9957.00	3846.39	17440.00	5918.96
92	1315.00	1201.63	14870.00	14122.33	28640.00	24146.67
125	686.30		10630.00		38210.00	
125	900.50	244.45	11890.00	2001.23	25600.00	7248.84
125	1174.00	920.27	14550.00	12356.67	25710.00	29840.00
155	941.70		11220.00		26100.00	
155	483.50	260.59	8224.00	1538.58	23260.00	6569.66
155	497.50	640.90	10330.00	9924.67	35790.00	28383.33
184	936.30		13330.00		22890.00	
184	1004.00	35.35	11390.00	1681.97	32180.00	6507.92
184	987.80	976.03	14740.00	13153.33	19640.00	24903.33
204	811.50		13760.00		24360.00	
204	873.20	54.85	13120.00	789.45	16430.00	4015.08
204	920.90	868.53	12190.00	13023.33	19300.00	20030.00
240	872.30		12970.00		19310.00	
240	513.30	263.11	6374.00	3537.89	37780.00	9238.26
240	1026.00	803.87	11890.00	10411.33	28120.00	28403.33
0	1.23		67.57		5876.00	
0	3.59		69.85		2896.00	
0	3.80	2.87	2.09	46.50	4563.00	4445.00
1	6.90		0.43		6153.00	
1	4.18		12.88		5576.00	
1	9.43	6.83	38.16	17.16	6832.00	6187.00
33	4.94		8.70		8657.00	
33	10.07		35.21		7794.00	
33	2.41	5.81	4.77	16.22	5787.00	7412.67
64	19.50		6.97		5656.00	
64	12.54		32.75		9997.00	
64	40.06	24.03	68.78	36.17	7766.00	7806.33
92	4.25		156.60		13730.00	
92	4.25		156.60		13730.00	
92	24.79	11.09	80.86	131.35	6675.00	11378.33
125	0.14		30.90		10830.00	
125	7.90		32.92		5231.00	
125	3.57	3.87	90.12	51.31	8298.00	8119.67
155	5.43		131.50		6559.00	
155	4.46		154.00		18020.00	
155	−0.89	3.00	84.31	123.27	19460.00	14679.67
184	0.37		153.90		18930.00	
184	2.32		202.30		22340.00	
184	0.15	0.95	185.50	180.57	18970.00	20080.00
204	7.68		117.00		16890.00	
204	0.48		19.95		9327.00	
204	18.04	8.73	96.94	77.96	13690.00	13302.33
240	−0.29		68.03		7577.00	
240	2.63		7.43		8056.00	
240	0.78	1.04	11.77	29.08	6106.00	7246.33

All elements are presented in ppb.